INT. J. NUM. METH. HEAT FLUID FLOW, VOL. 6, NO. 7, 47–62 (1996)

NUMERICAL STUDY OF THE EFFECTS OF ROTATIONAL BUOYANCY ON FULLY DEVELOPED FLOW IN ROTATING RECTANGULAR DUCTS

T. BO AND H. IACOVIDES

Mechanical Engineering Department, UMIST, Manchester M60 1QD, UK

ABSTRACT

This article examines the influence of centrifugal buoyancy on the hydrodynamic and thermal behaviour in fully developed flow through an orthogonally rotating duct of aspect ratio 2:1. A series of computations have been performed at rotation numbers ranging from 0 to 0.2, for constant-density flows (no buoyancy) and also for different levels of outward and inward buoyancy. The resulting comparisons reveal that for a Reynolds number of 32,500, rotational buoyancy effects become significant at Rayleigh number values greater than 10^7. In outward flows, buoyancy is found to strengthen the effects of the Coriolis force on the mean motion and, by raising turbulence levels, buoyancy also enhances wall heat transfer along both the pressure and the suction side of the rotating duct. In inward flows, it is found that strong buoyancy can reverse the direction of the Coriolis-induced secondary motion, which causes a strong rise in wall heat transfer along the suction side and a similarly significant fall in heat transfer along the pressure side. The computed effects on heat transfer are in qualitative agreement with the findings of a number of experimental studies. For both inward and outward flows, at a constant Reynolds number, the modifications of centrifugal buoyancy on the side-averaged levels of heat transfer correlate reasonably well with the rotational Rayleigh number.

KEY WORDS Duct flow Numerical computation Rotation Convective heat transfer Rotational buoyancy

NOMENCLATURE

$C_{\varepsilon 1}, C_{\varepsilon 2}, C_{\varepsilon 3}$	= Turbulence modelling constants
D	= Duct hydraulic diameter
h	= Surface coefficient of heat transfer ($= q_w/(\Theta_w - \Theta_B)$)
k	= Turbulent kinetic energy
l	= Equilibrium length scale
Nu	= Nusselt number ($= hD/\alpha$)
Nu_0	= Side-averaged Nusselt number for flow in a stationary duct
Nu_{rs}	= Side-averaged Nusselt number for constant-density flow in a rotating duct
P	= Pressure
P_k	= Generation rate of turbulence
P_{kB}	= Generation of turbulence owing to buoyancy
q_w	= Wall heat transfer rate per unit area
R	= Distance from the centre of rotation in Guidez's[8] experiments
Ra	= Rotational Rayleigh number ($= \Omega^2 D^4 X_3 q_w Pr/(\alpha \Theta_B)$)
Re	= Reynolds number ($= W_B D/\nu$)
Ro	= Rotation number ($= \Omega D/W_B$)
U_i	= Means velocity vector
U_τ	= Friction velocity
u_i	= Fluctuating velocity vector
W	= Streamwise velocity
W_B	= Bulk velocity
X_i	= Distance from the centre of location
X_3	= Streamwise distance from the centre of rocation
x_i	= Co-ordinate vector
Y	= Near-wall distance
y	= Co-ordinate direction normal to the symmetry plane
y^+	= Dimensionless near-wall distance ($= YU_\tau/\nu$)
y^*	= Dimensionless near-wall distance ($= Yk^{0.5}$)
z	= Streamwise co-ordinate
α	= Thermal conductivity
δ_{ij}	= Kroneker dhelta
ε	= Dissipation rate of turbulence
Θ	= Mean temperature
Θ_B	= Bulk temperature
θ	= Temperature fluctuation
λ	= Thermal diffusivity
μ	= Dynamic viscosity
ν	= Kinematic viscosity
ρ'	= Fluid density
ρ	= Density fluctuation
σ	= Turbulent Prandtl number
τ_w	= Wall shear stress
Ω_i	= Rotation vector

0961–5539

Received June 1995

INTRODUCTION

The effects of rotation on the hydrodynamic and thermal characteristics of internal flows have been the subject of many investigations, because of their importance to the design of internal cooling passages of gas-turbine blades. In addition to rotation, curvature and rib-roughness also influence the flow and thermal behaviour within blade cooling passages. In this study, attention is focused on only the effects of rotation, by examining fully-developed flows through straight ducts that rotate in an orthogonal mode, as shown in *Figure 1*.

In the isothermal flows through rotating ducts, only the Coriolis force influences the fluid motion, by creating a cross-duct pressure variation. When the fluid moves away from the centre of rotation (outward flow), the high pressure side coincides with the trailing side of the rotating duct, whereas in inward flows the pressure side is the leading side. A number of earlier theoretical investigations, such as Majumdar *et al.*[1], Howard *et al.*[2], Taylor *et al.*[3] and Iacovides and Launder[4], revealed that within the near-wall regions, the imbalance between the pressure gradient force and the Coriolis force drives the near-wall fluid from the pressure to the suction side, producing two symmetric secondary vortices as shown in *Figure 2(a)*. Studies of fully-developed

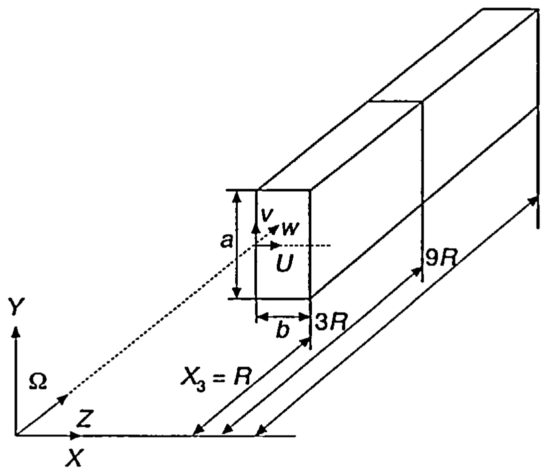

Figure 1 Flow geometry

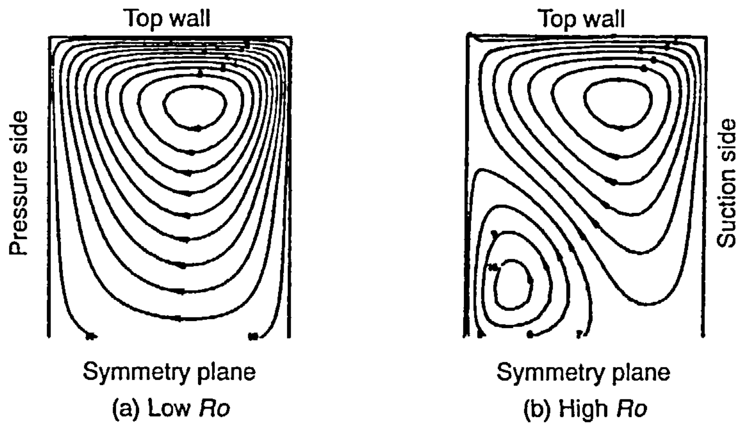

Figure 2 Coriolis-induced secondary motion

flow[4,5], have demonstrated that at higher rotation numbers ($Ro = \Omega D/W_B$), an extra pair of smaller, counter-rotating vortices is formed on the pressure surface, as shown in *Figure 2(b)*. Moreover, Iacovides and Launder[5] have shown that over a certain range of rotational speeds it is possible to predict either a two- or a four-vortex pattern depending on initial conditions. The Coriolis force also exerts a direct influence on the turbulence field[6] by augmenting turbulence mixing on the high pressure surface and impeding it on the suction surface. In three-dimensional rotating flows, however[4,6], the strongest influence on the flow development arises from the direct Coriolis effects on the mean motion. The above-mentioned numerical studies and also experimental investigations such as those of Wagner *et al.*[7] and Guidez[8], indicate that the secondary motion enhances heat transfer along the pressure wall and attenuates heat transfer levels along the suction side.

Inflows through strongly heated rotating ducts, large near-wall density gradients, combined with the centrifugal acceleration, bring an additional influence on the flow and thermal development, namely that of rotational buoyancy. In heated ducts, the centrifugal force is weaker within the near-wall regions, where the fluid is at a lower density. In outward flows, rotational buoyancy is consequently expected to slow down the near-wall fluid, leading to thicker boundary layers, while, for inward flow, it would accelerate the near-wall fluid, producing thinner boundary layers. In addition to its effects on the mean motion, as shown in the next section, rotational buoyancy also directly modifies turbulence.

While the primary effects of rotational buoyancy on the flow development can be easily deduced from the relevant flow equations, the question of how it further modifies the Coriolis-affected flow behaviour is a more difficult one to answer. Probably the first experimental study to distinguish decisively between Coriolis and buoyant effects was that of Wagner *et al.*[7]. It was shown that, for developing outward flow at a given rotation number, stronger heating rates led to higher heat transfer coefficients along both the pressure and the suction side. The suction side showed the stronger enhancement. In a subsequent experimental study from the same group[9], it was shown that rotational buoyancy also increases pressure and suction side heat transfer in developing inward flows. The buoyancy-related enhancement in heat transfer was not as strong as that observed in outward flows, but the inward flow measurements were influenced by the presence of a sharp U-bend at the start of the 12-diameter long straight section. Kuo and Hwang[10], on the other hand, found that, at Reynolds numbers less than 4,000 outward buoyancy reduced heat transfer levels, but at higher Reynolds numbers heat transfer levels were unaffected. For inward flows, Kuo *et al.*[11] found that rotational buoyancy increases the Nusselt number, a trend which is in agreement with that found by Wagner *et al.*[9], but which for the pressure side was opposite to the findings of Harasqama and Morris[12].

These experimental findings suggest that the effects of rotational buoyancy on heat transfer vary according to the combination of Reynolds, rotation and buoyancy number values. However, because of the absence of local flow measurements, it is not possible to gain a sufficiently detailed understanding of the effects of rotational buoyancy from the available experimental data. One of the first numerical studies to include the effects of rotational buoyancy for flow through rotating pipes[6], did show the expected effects on the boundary layer development. Subsequent studies of developing outward flows through rotating ducts, such as Prakash and Zerkle[13] and Bo *et al.*[14], have also included the effects of buoyancy and were able to reproduce the Wagner *et al.*[7] measurements with acceptable accuracy. By also performing constant-density computations for the same Reynolds and rotation numbers, Bo *et al.*[14] revealed that, at a rotational Rayleigh number value of 1.6×10^8, outward buoyancy modifies the predicted flow development and, as shown in *Figure 3*, causes a substantial increase in the heat transfer levels along the pressure side. It was thus demonstrated that numerical methods can capture the main features of flows influenced by rotational buoyancy.

In this study, the effects of rotational buoyancy (outward and inward) are examined in greater detail, by concentrating on fully-developed flow through a rotating duct of aspect ratio of 2:1. The Reynolds number is kept constant at 32,500 and the rotation number varies from 0 to 0.2. At each

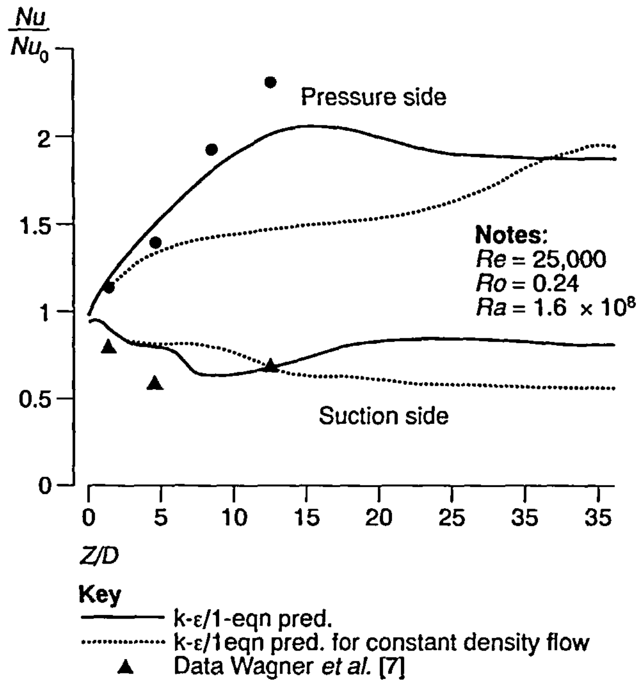

Figure 3 Development of the side-averaged Nusselt number in outward flow through a square rotating duct, from Bo *et al.*[14]

rotation number, seven predictions have been obtained; one without buoyancy (constant density), three at different levels of outward buoyancy and three further computations at similar levels of inward buoyancy. The objective is to examine how rotational buoyancy further modifies flow and heat transfer in rotating ducts. Consideration is given to the detailed flow structure, the turbulence field and also to the local and side-averaged Nusselt numbers.

THE MATHEMATICAL MODEL

The mean flow field

The Reynolds equations describing the motion of turbulent flow in a rotating co-ordinate system may be written as :

$$\frac{\partial}{\partial x_j}\left(\rho U_i U_j\right) = -\frac{\partial P}{\partial x_i} + \frac{\partial}{\partial x_j}\left[\mu\left(\frac{\partial U_i}{\partial x_j}+\frac{\partial U_j}{\partial x_i}\right) - \rho\overline{u_i u_j}\right] - 2\rho\,\varepsilon_{ijl}\Omega_j U_l$$

$$-\rho\left(\Omega_j X_j \Omega_i - \Omega_j X_i \Omega_j\right)$$

where Ω_i denotes the rotation vector and X_i the distance from the centre of rotation. In this case, U_3 (W) represents the streamwise velocity and Ω_2 is the only non-zero component of the rotation vector. The third term on the right-hand side of the momentum transport equation represents the Coriolis force and the fourth term the centrifugal force. In constant density flows, the centrifugal force is uniform across the duct and it is counteracted by an also uniform pressure gradient force. In heated flows ,on the other hand, because of cross-duct variations in density, the centrifugal force is no longer uniform and therefore cannot be cancelled by the still uniform pressure gradient.

The continuity equation is expressed as:

$$\frac{\partial}{\partial x_j}(\rho U_j) = 0$$

The local density ρ is related to the mean temperature Θ through :

$$\rho = \rho_o \Theta_o / \Theta$$

The temperature is obtained from the energy equation:

$$\frac{\partial}{\partial x_j}\left(\rho U_j \Theta\right) = \frac{\partial}{\partial x_j}\left(\lambda \frac{\partial \Theta}{\partial x_j} - \rho \overline{u_j \theta}\right)$$

where λ is the thermal diffusivity obtained from $\lambda = \mu / Pr$.

Turbulence modelling

In initial flow computations in rotating ducts, Majumdar *et al.*[1] employed the high-*Re* k-ε model with the semi-logarithmic wall laws (wall-functions) used to bridge the wall sub-layer. In computations of flows through stationary curved ducts, which are dominated by similar secondary flow patterns, Choi *et al.*[15] also Besserman and Tanricut[16] abandoned the wall-function approach and integrated the momentum equations across the wall sub-layer. Simple near-wall models such as the Van-Driest[17] mixing length were used, matched to high-*Re* models like the k-ε in the duct core. This zonal modelling approach was found able to resolve the secondary motion with greater accuracy, producing more reliable flow and heat transfer predictions. The same near-wall modelling practice was then successfully employed in computations of rotating flows by Taylor *et al.*[3] and Iacovides and Launder[4,6]. For isothermal flows, attempts to take into account the direct Coriolis effects on the turbulence field, either within an effective viscosity or a stress closure[2,4,6] did not significantly alter the resulting predictions.

In this study, a zonal effective-viscosity model was therefore employed, in which the high-*Re* k-ε model in the duct core was coupled to a low-*Re* one-equation model of k-transport in the near-wall regions. As can be seen in *Figure 3*, our earlier studies of developing outward flow through a rotating duct[14] have shown that this model is able to reproduce the thermal development observed by Wagner *et al.*[7] with sufficient accuracy.

In both regions, the turbulent stresses and heat fluxes are obtained through the effective-viscosity approximation:

$$\overline{u_i u_j} = \frac{2k}{3}\delta_{ij} - \mu_t\left(\frac{\partial U_i}{\partial x_j} + \frac{\partial U_j}{\partial x_i}\right) \qquad \overline{u_i \theta} = -\frac{\mu_t}{\sigma_\theta}\frac{\partial \Theta}{\partial x_i}$$

where σ_Θ is the temperature turbulent Prandtl number.

In the k-ε model, the turbulent viscosity, μ_t, is obtained from the turbulent kinetic energy, k, and its dissipation rate, ε, according to:

$$\mu_t = \rho c_\mu k^2/\varepsilon$$

The transport equations for k and ε are as follows:

$$\frac{\partial}{\partial x_j}\left(\rho U_j k\right) = \frac{\partial}{\partial x_j}\left[\left(\mu + \frac{\mu_t}{\sigma_k}\right)\frac{\partial k}{\partial x_j}\right] + P_k - \rho \_$$

$$\frac{\partial}{\partial x_j}\left(\rho U_j \varepsilon\right) = \frac{\partial}{\partial x_j}\left[\left(\mu + \frac{\mu_t}{\sigma_\_}\right)\frac{\partial \varepsilon}{\partial x_j}\right] + c_{\varepsilon 1}\frac{\varepsilon}{k}P_k - \rho c_{\varepsilon 2}\frac{\varepsilon^2}{k}$$

The generation rate of the turbulent kinetic energy, P_k, is obtained from:

$$P_k = \mu_t \frac{\partial U_i}{\partial x_j}\left(\frac{\partial U_i}{\partial x_j} + \frac{\partial U_j}{\partial x_i}\right) - \frac{\overline{\rho' u_i}}{\rho}\left(\Omega_i X_j \Omega_j - \Omega_j X_j \Omega_i\right)$$

The second contribution to the generation rate term represents the direct effects of rotational buoyancy on turbulence. In ideal gases:

$$\frac{\overline{\rho' u_i}}{\rho} = -\frac{\overline{\theta u_i}}{\Theta}$$

With the introduction of the effective diffusivity approximation, the generation rate therefore becomes:

$$P_k = \mu_t \frac{\partial U_i}{\partial x_j}\left(\frac{\partial U_i}{\partial x_j} + \frac{\partial U_j}{\partial x_i}\right) - \frac{\mu_t}{\Theta\sigma_\theta}\frac{\partial \Theta}{\partial x_i}\left(\Omega_i X_j \Omega_j - \Omega_j X_j \Omega_i\right)$$

For a duct rotating in orthogonal mode, with Ω_2 (= Ω) the only non-zero component, the contribution of buoyancy to P_k becomes :

$$P_{kB} = \frac{\mu_t}{\Theta\sigma_\theta}\left(\Omega^2 X_1 \frac{\partial \Theta}{\partial x_1} + \Omega^2 X_3 \frac{\partial \Theta}{\partial x_3}\right)$$

The second term in P_{kB} is always positive in outward flows and negative in inward flows. In eccentrically rotating ducts, the first term in P_{kB} would have opposite signs on the leading and trailing sides of the rotating duct. Because the streamwise distance from the centre of rotation, X_3, is greater than the cross-duct distance X_1, the buoyant generation rate related to the cross-duct distance may not be very significant.

In the near-wall one-equation model, the transport equation for k is the same as that of the k-ε model. The dissipation rate ε is obtained from the near-wall distance, Y, according to Wolfstein's[18] proposal:

$$\varepsilon = k^{1.5}/l_\varepsilon$$

where

$$l_\varepsilon = 2.4Y\{1 - \exp(-0.236y^*)\}.$$

The dimensionless near-wall distance y^* is defined as:

$$y^* = Yk^{0.5}/\nu.$$

The turbulent viscosity, μ_t is obtained from:

$$\mu_t = c_\mu \rho\, l_\mu k^{0.5}$$

where

$$l_\mu = 2.4Y\{1 - \exp(-0.016y^*)\}.$$

The turbulence modelling constants that appear in the above equations have the values given in the *Table 1*.

Table 1 Turbulence modelling constants

$c_{\varepsilon 1}$	$c_{\varepsilon 2}$	c_μ	σ_k	σ_ε	σ_Θ
1.44	1.92	0.09	1	1.22	0.9

NUMERICAL ASPECTS

A finite-volume numerical solver, described in earlier publications[4], has been used in this investigation. The staggered grid approach is employed and conservation of mass and momentum is ensured through the integration of the transport equations over each control volume. Because only fully-developed flows are investigated, the numerical procedure is two-dimensional, but it involves the solution of three velocity components. All gradients in the streamwise direction are assumed to be zero, apart from the pressure and temperature gradients, which are assumed to be uniform across the duct and are determined from the overall mass and energy balance respectively. Further details can be found in Bo[19].

Owing to the flow symmetry, only half the duct cross-section needs to be considered, with symmetry boundary conditions at $y = 0$. The use of a low-Reynolds-number model in the near-wall regions, enables the application of no-slip wall-boundary conditions. For the enthalpy equation, constant wall heat flux boundary conditions are imposed.

A non-uniform mesh was employed, consisting of 67 nodes between the pressure and suction walls and 45 nodes between the plane of symmetry and the top wall. The first ten near-wall nodes were located within the low-Reynolds-number one-equation region. The value of y^+ ($= YU_\tau/\nu$) at the wall-adjacent nodes was always less than three. This ensures that these nodes are within the viscosity-dominated sub-region where turbulent stresses are negligibly small. At the interface between the two- and the one-equation regions, the y^+ values ranged between 80 and 120.

PRESENTATION AND DISCUSSION OF RESULTS

In all the computations presented, the flow Reynolds number was kept constant at 32,500, which coincides with that in Guidez's[8] experimental study of developing outward flow in a rotating duct of identical aspect ratio. Initially six constant-density flow computations were obtained, for rotation number values up to 0.2, in order to first establish how the Coriolis force alone affects the flow development. Variable density computations were subsequently performed at the same rotation numbers. In all cases, the fluid bulk temperature was maintained at the same level. As mentioned earlier, three sets of outward and three sets of inward flows were predicted over the same rotation number range. For each group of buoyant flow predictions, the streamwise distance from the centre of rotation, X_3 was kept constant, as a result of which as the rotational Rayleigh number increased with the rotation number. In the first group of computations, X_3 was set equal to R, where R is the distance required to reproduce the Rayleigh numbers of the flows examined in Guidez's[8] study. The streamwise distance from the centre of rotation was subsequently increased to $3R$ and $9R$, providing two further sets of computations over the same range of rotation number, but at higher levels of rotational buoyancy. All the combinations of rotation and Rayleigh numbers computed are summarized in *Table 2*. For most of the cases listed in *Table 2*, two solutions have been obtained; one in which the initial conditions were those of uniform flow in a stationary duct

Table 2 Cases examined

	Outward flow				Inward flow		
	$X_3 = 9R$ $Ra/10^6$	$X_3 = 3R$ $Ra/10^6$	$X_3 = R$ $Ra/10^6$	Ra	$X_3 = R$ $Ra/10^6$	$X_3 = 3R$ $Ra/10^6$	$X_3 = 9R$ $Ra/10^6$
$Ro = 0.0053$	0.25	0.085	0.028	0	0.027	0.082	0.24
$Ro = 0.0266$	5.7	1.9	0.64	0	0.61	1.8	5.5
$Ro = 0.053$	23	7.3	2.4	0	2.3	7	21
$Ro = 0.075$	41	14	4.6	0	4.4	13	42
$Ro = 0.1088$	83	28	9.5	0	9.1	27	88
$Ro = 0.2$	250	89	30	0	30	94	290

and one in which starting conditions were obtained from a solution at a rotation number high enough for a four-vortex structure (*Figure 2(b)*) to exist. In this article, owing to space limitations, only the latter set of computations is presented.

Figures 4 and *5* show the effects of rotational buoyancy on the mean motion. Secondary velocity streamlines and axial velocity contours predicted at constant density are compared with

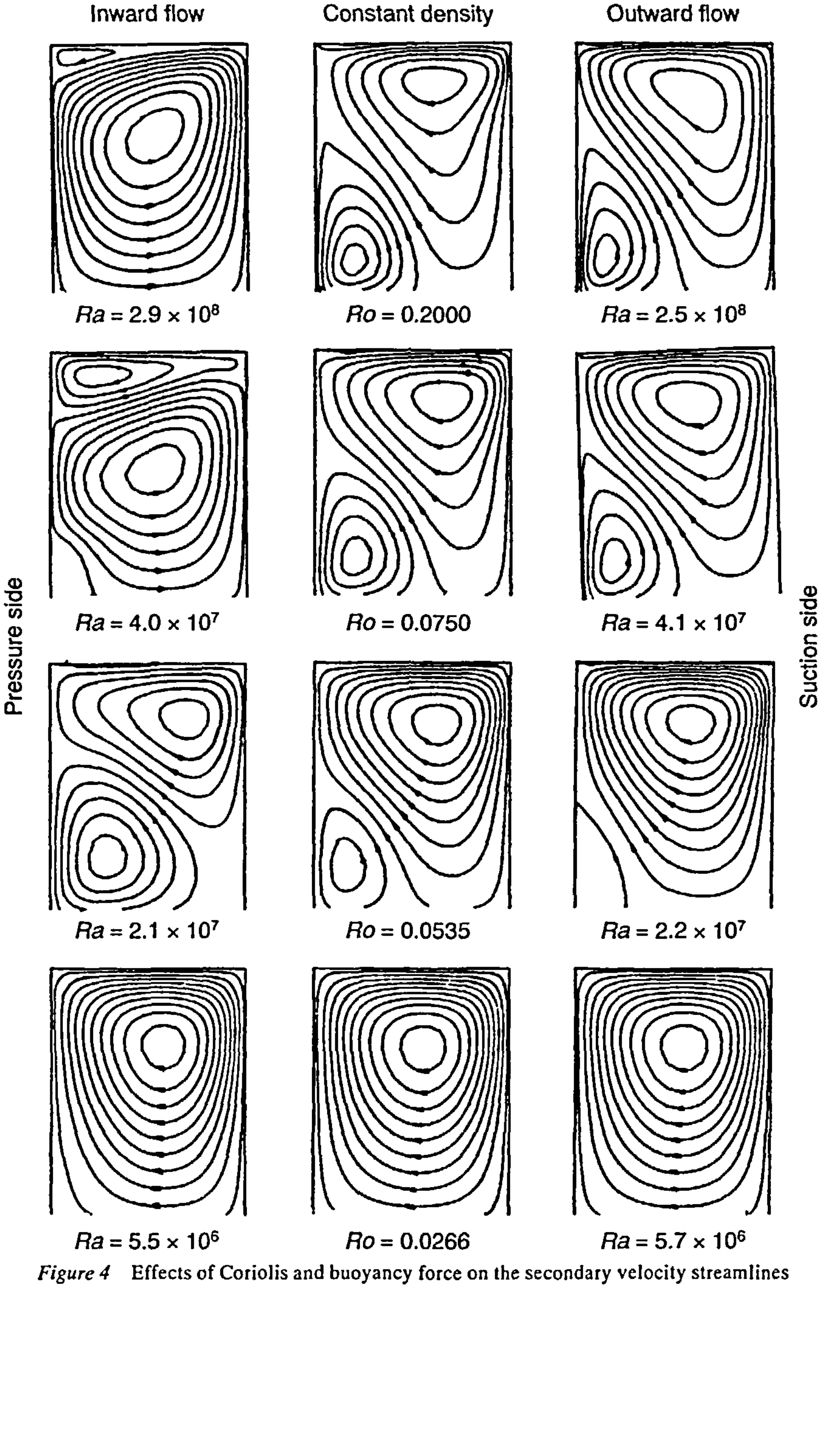

Figure 4 Effects of Coriolis and buoyancy force on the secondary velocity streamlines

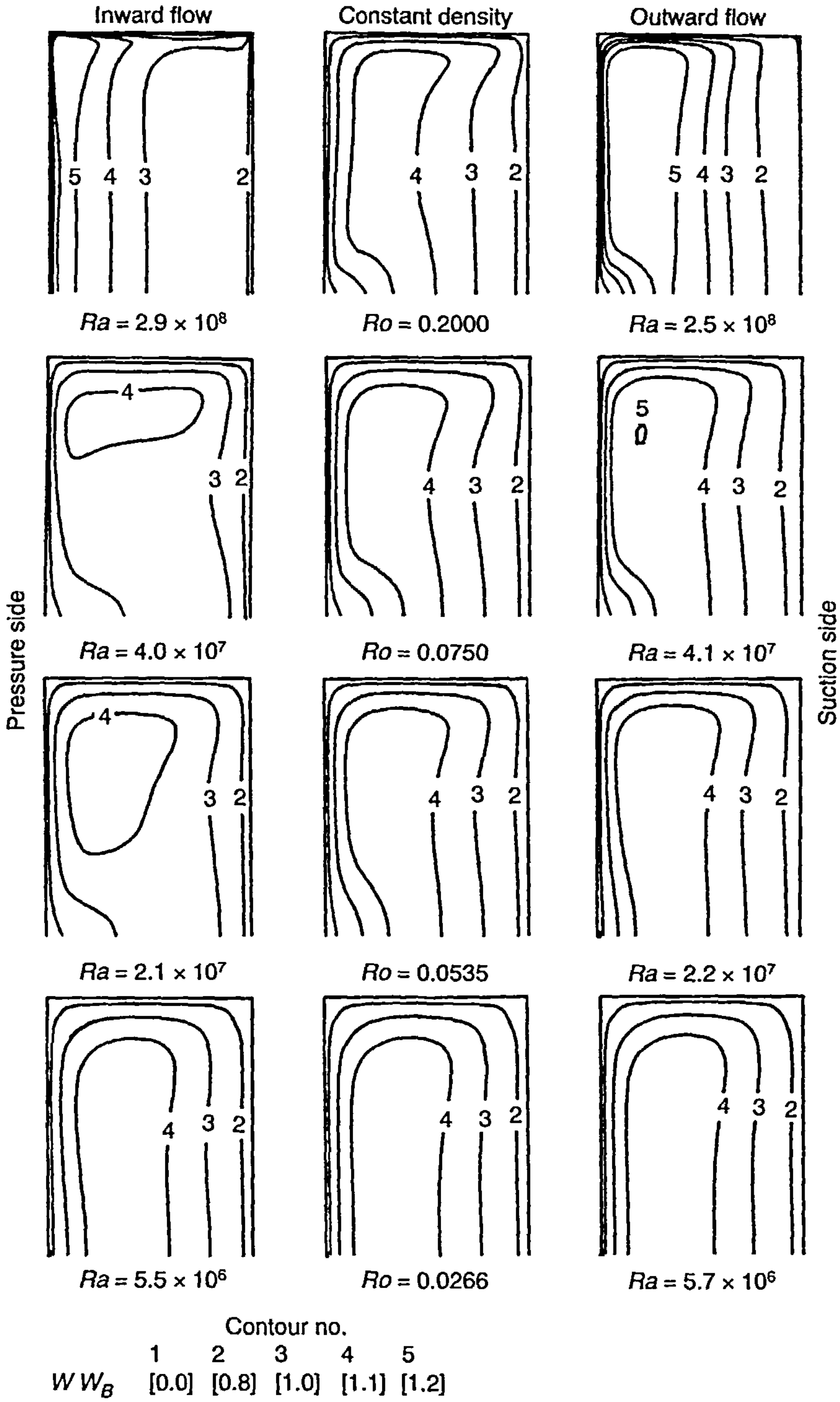

Figure 5 Effects of Coriolis and buoyancy force on the streamwise velocity contours

those computed for outward and inward buoyant flows, at $X_3 = 9R$, at the same rotation numbers. The constant density predictions display the behaviour revealed in the earlier study of Iacovides and Launder[5], in which the Coriolis force generates a secondary motion that transports the high momentum fluid towards the pressure side. Low momentum fluid is convected to the suction side and, as the Coriolis force becomes stronger, the pressure and top wall boundary layers become thinner. The counter-rotating vortices along the pressure side (on either side of the symmetry plane) disappear at rotation numbers lower than 0.05. Outward buoyancy, while not changing the overall character of the flow, appears to shift the high momentum fluid further towards the pressure side, causing a greater accumulation of low momentum fluid along the suction side and even thinner boundary layers along the pressure and top walls. This must be caused by the fact that the decelerating buoyant force is stronger along the suction side of the duct, where most of the hotter fluid accumulates, owing to the action of the Coriolis-induced secondary motion. Continuity therefore dictates that, as fluid along the suction side is slowed down, the flow velocity along the pressure half of the duct must increase in order to preserve the same overall flow rate. The same reason probably also accounts for the fact that, in the case of outward flow, the lower *Ro* limit at which the counter-rotating vortices can be sustained is increased. At a distance of $9R$ from the centre of rotation, rotational buoyancy effects first become significant at *Ro* values above 0.05, which correspond to Rayleigh number values greater than 2.2×10^7.

Inward buoyancy, on the other hand, causes more substantial changes in the flow behaviour. As the effects of buoyancy become significant (for $Ra > 2 \times 10^7$), the boundary layer along the suction side, where as already noted the fluid is hotter, becomes thinner and the cooler fluid at the centre of the duct is now slowed down by the buoyancy force. As a result, the high momentum fluid is pushed towards the top wall, where fluid temperatures are higher. As buoyancy becomes progressively stronger, the faster moving fluid is pushed right up against the top surface. Because the core fluid is slowed down, the Coriolis force over this region weakens and the counter-rotating vortex along the pressure side becomes larger. At $Ro = 0.2$ and $Ra = 2.9 \times 10^8$, the counter-rotating vortex expands to occupy almost the entire symmetric half of the duct's cross-section, effectively reversing the secondary motion. (The computations with stationary initial conditions show an abrupt reversal in the secondary motion at a Rayleigh number greater than 10^8.) The faster fluid which is now closer to the top wall, is driven from the suction to the pressure side. The fluid then returns to the suction side through the duct centre. The interaction between the buoyant and the Coriolis force has thus led to a flow field that is markedly different from that generated by the Coriolis force alone.

The effects of rotational buoyancy on the turbulence field are illustrated in *Figure 6*, in which cross-duct profiles of turbulence intensity at *Ro* values of 0.1088 and 0.2, at $X_3 = 9R$, are compared with the corresponding constant-density profiles. In the absence of buoyancy, the turbulence levels are fairly uniform across the duct, showing only a modest rise near the pressure-side wall, where the secondary motion transports core fluid to the near-wall regions. Outward buoyancy raises turbulence levels over most of the duct cross-section, but especially along the suction side, reversing the trend observed in the isothermal case. As can be seen in *Figure 6(b)*, these effects become stronger at higher Rayleigh numbers. Since outward buoyancy does not alter the overall mean flow behaviour, this marked increase in turbulence levels must be attributed to the direct effects of buoyancy on turbulence, which have been described earlier. Inward buoyancy, appears to have a less pronounced effect on the predicted turbulence levels. At Rayleigh numbers less than 10^8 (*Figure 6(c)*), its main effect appears to be a modest reduction in the core turbulence levels. At higher Rayleigh numbers, as shown in *Figure 6(d)*, the suction side turbulence levels become lower than those of the constant density field, while along the pressure side they begin to increase. These changes in the predicted distribution of turbulence levels result from the different mean flow features, generated by inward buoyancy and also from the direct effects inward buoyancy on turbulence.

The next question that now needs to be addressed is how these buoyancy-induced changes to the flow characteristics modify wall heat transfer. The effects on the local Nusselt number are

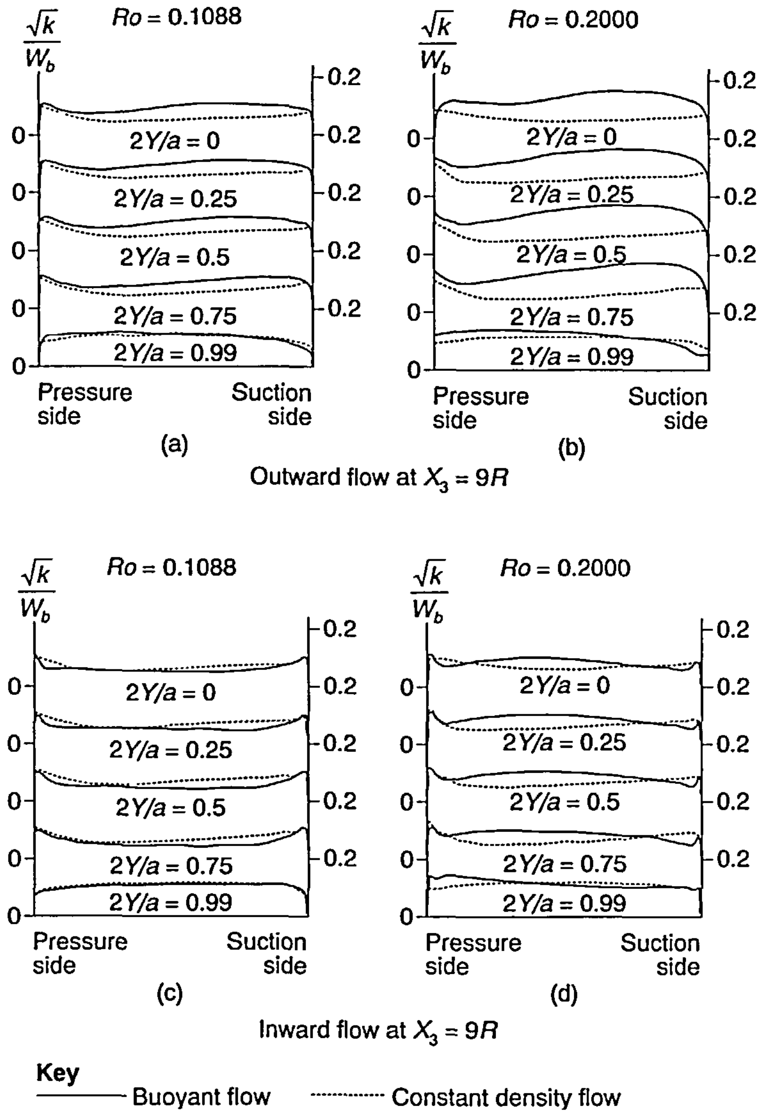

Figure 6 Profiles of turbulence intensity

displayed in *Figure 7*, where the Nusselt number distribution for outward and inward flows at $X_3 = 9R$, is compared with that for constant-density flows at the same rotation numbers. Along each side, Nusselt number values are normalized with the corresponding average value for fully-developed flow in a stationary duct, in order to highlight the effects of rotation. As pointed out by Iacovides and Launder[5], in the case of constant-density flow the Coriolis force leads to a substantial enhancement in the pressure and top-side heat transfer levels (60 per cent and 100 per cent respectively), while the suction-side wall heat transfer is reduced by as much as 20 per cent. This is consistent with the Coriolis effects on the mean flow. The effects of the counter-rotating vortex on the Nusselt number distribution along the pressure side are also clearly evident. As also noted in the mean flow comparisons, buoyancy effects become noticeable at *Ra* values greater

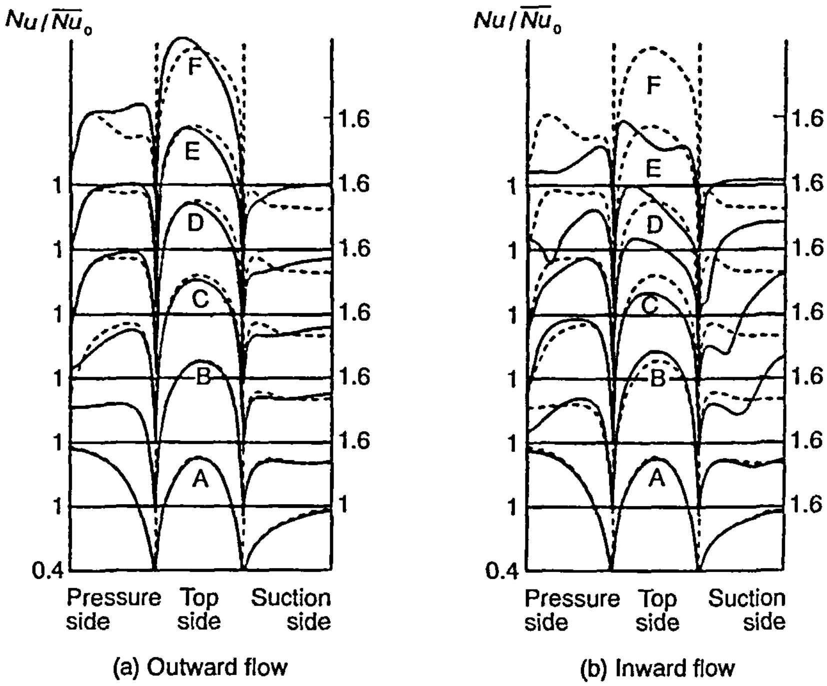

Key
——— Buoyant flow ··········· Constant density flow

Notes:
A: $Ro = 0.053$ B: $Ro = 0.0266$ C: $Ro = 0.0535$
D: $Ro = 0.075$ E: $Ro = 0.1088$ F: $Ro = 0.2000$

Figure 7 Variation of local Nusselt number with rotation and Rayleigh number at $X_3 = 9R$

than 2×10^7. Outward buoyancy appears to enhance the suction-side heat transfer rates significantly and some increase in wall heat transfer is also observed along the pressure side. Outward buoyancy effects on the top-side heat transfer rates appear to be minor. Since thicker boundary layers (which outward buoyancy causes to develop along the suction side) are normally associated with lower rates of wall heat transfer, the increase in heat transfer must be caused mainly by the higher turbulence levels produced in outward flows. This explanation is further supported by the fact that outward buoyancy has a stronger effect on heat transfer along the suction side where its effects on turbulence are also stronger. As expected, given the earlier mean flow comparisons, inward buoyancy has a stronger effect on the thermal behaviour. It appears to enhance wall heat transfer along the suction side significantly, but it also causes similarly strong reductions in wall heat transfer along the pressure and top sides. The main cause of this behaviour appears to be the reversal in the secondary motion, which now carries the cooler core fluid to the suction side and the hotter near-wall fluid from the suction side to the top- and pressure-side near-wall regions. The thinner boundary layer along the suction side also contributes to the increase in wall heat transfer over this side.

For outward buoyancy, the predicted heat transfer behaviour is in qualitative agreement with that observed in the Wagner *et al.*[7] experiments while, for inward buoyancy, the trends found agree with those identified in the Harasqama and Morris[12] experiments. As mentioned earlier, the alternative findings in other experiments may be caused by differences in the values of Reynolds, rotation and Rayleigh numbers and also by the developing nature of the experimentally investigated flows.

The effects of rotation on the side-averaged Nusselt numbers, for the pressure and suction sides, are shown in *Figure 8*. All the outward flow results are displayed in *Figure 8(a)* and inward

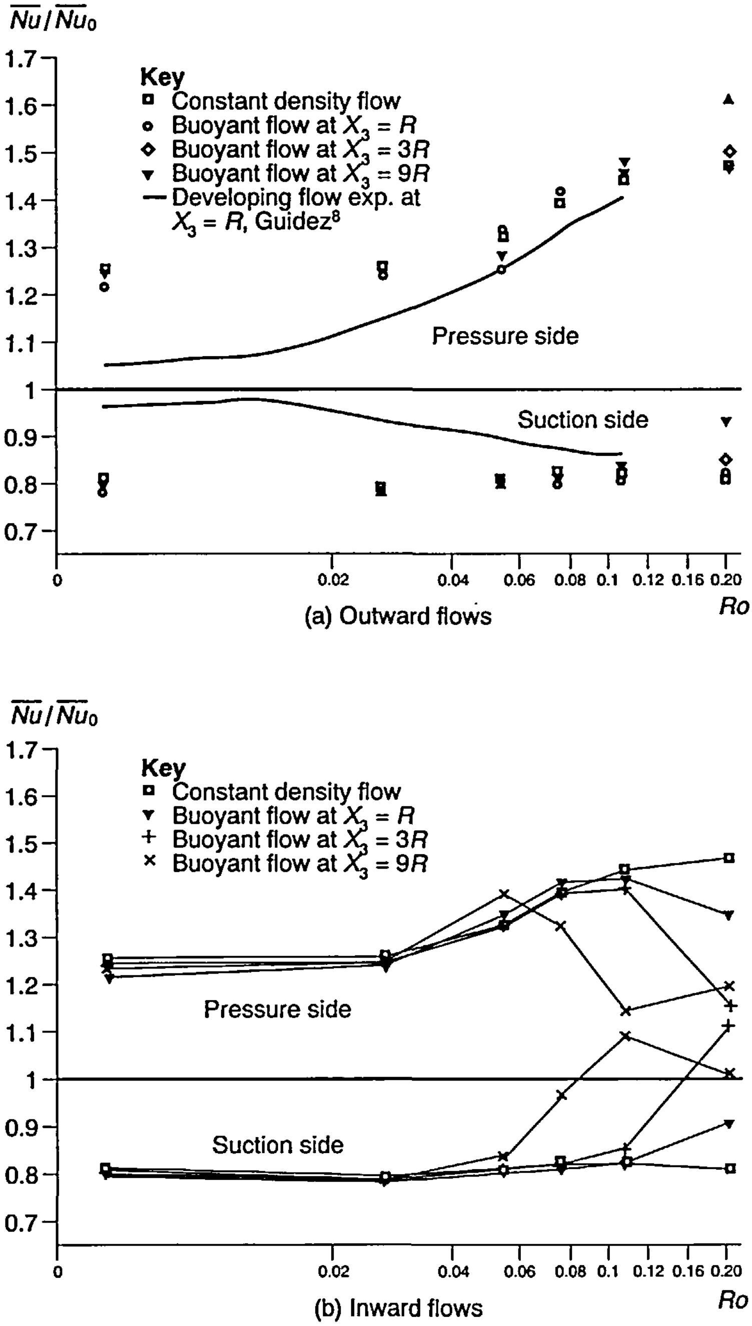

Figure 8 Variation of side-averaged Nusselt number with rotation and Rayleigh number

flow computations are shown in *Figure 8(b)*. As in *Figure 7*, Nusselt number values are normalized with the corresponding stationary value. In the outward flow comparisons, the measurements of Guidez[8] are also displayed. Guidez's measurements have been obtained at Rayleigh number values similar to those in the present computations with $X_3 = R$. The measurements have, however, been obtained for developing outward flow, with only about 7.4 diameters of flow development. These comparisons indicate that, at low rotation and Rayleigh numbers, outward buoyancy causes a modest reduction in heat transfer levels along both sides, but as the rotational speed increases the effect is reversed. This non-monotonic effect of outward buoyancy on heat transfer may provide the explanation for some of the contradictory findings that have emerged from earlier experimental studies. At high rotation numbers, it is evident that, as the distance from the centre of rotation (X_3) is increased, the effects of buoyancy at a particular rotation number become stronger. Guidez's[8] measurements show a similar thermal behaviour, but the effects of rotation are not as strong as in the computations, especially at the lower rotation numbers. These differences between the computed and the measured behaviour appear to arise from the developing nature of the measured flow. At higher rotation numbers, where the secondary motion is stronger, the length of flow development becomes shorter and consequently conditions after 7.4 diameters are closer to fully-developed, accounting for the closer accord between computations and measurements over this range. The corresponding comparisons for inward flow, *Figure 8(b)*, again confirm the strong effects of inward buoyancy on heat transfer. As the distance from the centre of rotation increases, the effects of buoyancy extend to lower rotation numbers, indicating that at a given Reynolds number the strength of buoyancy is determined by the Rayleigh number.

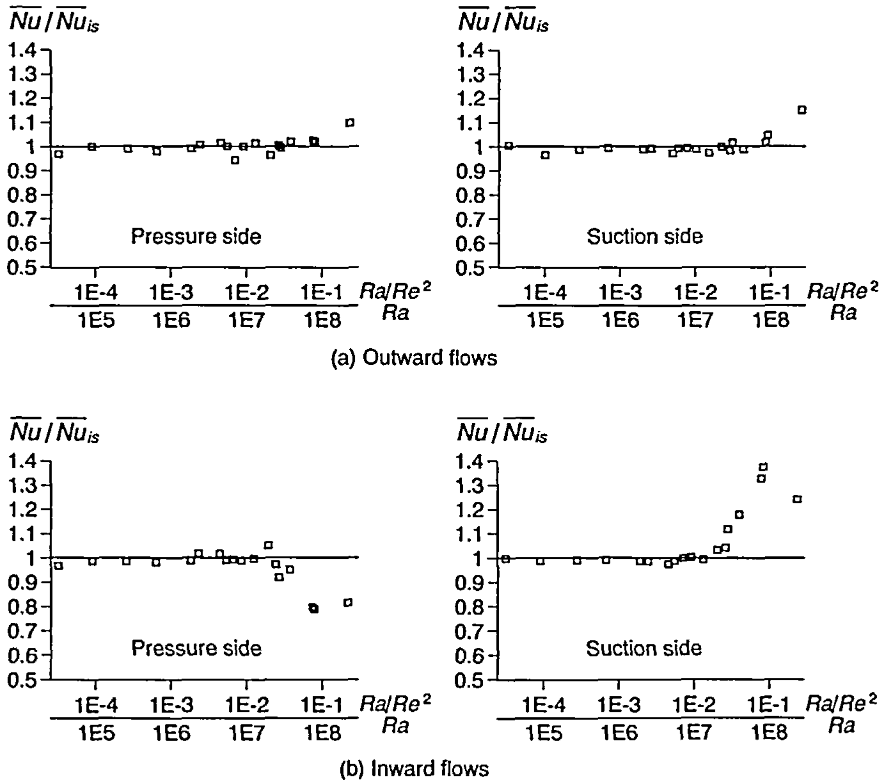

Figure 9 Effects of rotational buoyancy on the side-averaged Nusselt number

Finally, in an attempt to separate the effects of rotational buoyancy on heat transfer from those of the Coriolis force, in *Figure 9* the side-averaged Nusselt numbers for buoyant flows are normalized with the corresponding values for constant-density flows at the same rotation number and are then plotted against the rotational Rayleigh number. In addition to the Rayleigh number values, the x-axis also shows the values of Ra/Re^2 in order to minimize the Reynolds number effect. For both flow directions, the buoyant effect on heat transfer rates, at different rotation numbers, appears to correlate reasonably well with the Rayleigh number. In outward flow, at Rayleigh numbers below 10^7 (Ra/Re^2 of 0.01), buoyancy effects cause a modest reduction in heat transfer along both the pressure and the suction side. At higher Ra values, first the suction side and then the pressure side heat transfer coefficients begin to rise. At a value of Ra/Re^2 of 0.2, outward buoyancy raises wall heat transfer by about 12 per cent along the pressure side and by about 18 per cent along the suction side. In inward flows, buoyancy effects also become significant. The strongest effects of inward buoyancy on wall heat transfer occur at a value of Ra/Re^2 of 0.1. At the suction side, the constant-density Nusselt number is increased by 40 per cent, while at the pressure side it is reduced by 20 per cent. The effects of inward buoyancy on wall heat transfer begin to diminish at Ra/Re^2 values higher than 0.1. One possible explanation is that, beyond this Ra level, as shown in *Figure 6(d)*, inward buoyancy also starts to influence near-wall turbulence. These buoyancy-related modifications to the turbulence field have the opposite effect on heat transfer to those of the mean flow field. Owing to the lack of a sufficient number of numerical data over this range, no definitive conclusions can however be drawn on this issue.

CONCLUSIONS

This study, probably for the first time, has revealed in detail how centrifugal buoyancy influences the hydrodynamic and thermal behaviour in rotating ducts. Owing to the non-linear nature of the laws of fluid motion, the interaction between the buoyant and Coriolis forces results in modifications to the flow and heat transfer which cannot be deduced by simply considering the primary effects of centrifugal buoyancy on the mean and the fluctuating motion. For a constant flow Reynolds number, the modifications that rotational buoyancy produces to the Coriolis-affected levels of side-averaged wall heat transfer, appear to correlate reasonably well with the rotational Rayleigh number. At a Reynolds number of 32,500, rotational buoyancy effects become noticeable at a Rayleigh number of 10^7 or at an Ra/Re^2 level of 0.01.

In outward flows, on the whole rotational buoyancy enhances the effects of the Coriolis force on the mean flow, by moving the faster fluid closer to the pressure side and by enlarging the region of low momentum fluid along the suction side. Turbulence levels are increased by outward buoyancy over the entire cross-section, but especially along the suction side, where they reach their maximum levels. As a result, the levels of heat transfer are also increased relative to those at constant-density, especially along the suction side, where at an Ra/Re^2 value of 0.2, outward buoyancy enhances average wall heat transfer by almost 20 per cent.

Inward buoyancy is found to exert a greater influence on flow and heat transfer. By reducing the streamwise velocity at the duct centre, while accelerating the near-wall flow, inward buoyancy eventually leads to the reversal in the direction of the Coriolis-induced secondary motion. This change in the secondary flow leads to a substantial increase in the levels of heat transfer along the suction side and to an equally strong reduction in wall heat flux at the pressure side. When Ra/Re^2 becomes 0.1 the suction-side heat transfer is increased by 40 per cent and along the pressure side it is reduced by 20 per cent. At higher levels of inward buoyancy, there is some evidence that changes to the turbulence field begin to counteract the effects of the mean motion on heat transfer.

The computed heat transfer behaviour is in qualitative accord with that found in some of the available experimental studies. Computations over a wider range of Reynolds, rotation and Rayleigh numbers are however necessary, before a fuller picture can emerge on how the Nusselt number depends on Reynolds, rotation and Rayleigh numbers.

ACKNOWLEDGEMENTS

This research has been supported by Rolls-Royce plc and DRA/Pyestock, under Research Brochure B1D2-125D. The authors would also like to acknowledge Professor B.E. Launder's advice and encouragement during the course of this work.

REFERENCES

1 Majumdar, A.K., Pratap, V.S. and Spalding, D.B., Numerical computation of flow in rotating ducts, *ASME J. Fl Engrg*, **99**, 148-153 (1977)
2 Howard, J.H.G., Patankar, S.V. and Bordynulk, R.M., Flow prediction in rotating ducts using Coriolis-modified turbulence models, *ASME J. Fl Engrg*, **102**, 456-461 (1980)
3 Taylor, C., Rance, C. and Medwell, J.O., A method for the prediction of Coriolis-induced secondary flows and their influence on heat transfer in rotating ducts, *Engrg Comput*, **2**, 2-12 (1985)
4 Iacovides, H. and Launder, B.E., Turbulent momentum and heat transport in square cross-sectioned ducts rotating in orthogonal mode, *Num. Heat Tr.*, **12**, 475-491 (1987)
5 Iacovides, H. and Launder, B.E., Parametric and numerical study of fully-developed flow and heat transfer in rotating rectangular ducts, *ASME J. of Turbomachinery*, **113**, 331-338 (1991)
6 Iacovides, H. and Launder, B.E., Numerical simulation of flow and heat transfer in tubes in orthogonal mode rotation, *Proc. 6th Int. Symp. on Turb. Shear Flows*, Toulouse, France (1987)
7 Wagner, J.H., Johnson, B.V. and Hajek, T.J., Heat transfer in rotating passages with smooth walls, *ASME Paper 89-GT-172, Int. Gas-Turb. & Aero Congress*, Ontario (1989)
8 Guidez, J., Study of the convective heat transfer in a rotating coolant channel, *ASME J. Turbomachinery*, **111**, 43-50 (1989)
9 Wagner, J.H., Johnson, B.V. and Kooper, F.C., Heat transfer in a rotating serpentine passage with smooth walls, *ASME J. Turbomachinery*, **113**, 231-330 (1991)
10 Kuo, C.R. and Hwang, G.J., Aspect ratio effect on convective heat transfer of radially outward flow in rotating rectangular ducts, *Int. J. of Rot. Machinery*, **1**, 1-18 (1994)
11 Kuo, C.R., Chen, J.L. and Hwang, G.J., Experimental study of convective heat transfer in a radially rotating square duct with uniform wall heat flux and inward flow, *ASME Paper 93-WA/HT-54, ASME Winter Annual Meeting*, New Orleans, Louisiana (1993)
12 Harasqama, S.P. and Morris, W.D., The influence of rotation on the heat transfer characteristics of circular, triangular and square-sectioned coolant passages of gas-turbine rotor blades, *ASME J. Turbomachinery*, **110**, 44-50 (1988)
13 Prakash, C. and Zerkle, R., Prediction of turbulent flow and heat transfer in a radially rotating square duct, *ASME J. Turbomachinery*, **114**, 835-845 (1992)
14 Bo, T., Iacovides, H. and Launder, B.E., The prediction of convective heat transfer in rotating square ducts, *8th Int. Symp. on Turb. Shear Flows*, Munich, Germany (1991)
15 Choi, Y-D., Iacovides, H. and Launder, B.E., Numerical computation of turbulent flow in a square-sectioned 180° bend, *ASME J. Fl Engrg*, **111**, 59-68 (1989)
16 Besserman, D.L. and Tanrikut, S., Comparison of heat transfer measurements with computations for turbulent flow around a 180° bend, *ASME paper 92-GT-2, Int. Gas-Turb. & Aero. Congress*, Orlando (1991)
17 Van-Driest, E.R., On turbulent flow near a wall, *J. of Aero. Soc.*, **23**, 1007 (1956)
18 Wolfstein, M., The velocity and temperature distribution in one-dimensional flow with turbulence augmentation and pressure gradient, *Int J Heat Mass Transfer*, **12**, 301-318 (1969)
19 Bo, T., The computation of flow and heat transfer in rotating ducts and U-bends, PhD thesis, Dept. of Mesh Engrg, Faculty of Technology, University of Manchester.